minerals

MDPI

Article

Mineralogy and Mineral Chemistry of the Au-Ag-Te-(Bi-Se) San Luis Alta Deposit, Mid-South Peru

Pura Alfonso [1,*], Elsa Ccolqque [1], Maite Garcia-Valles [2], Arnau Martínez [1], Maria Teresa Yubero [1], Hernan Anticoi [1] and Nor Sidki-Rius [1]

[1] Departament d'Enginyeria Minera, Industrial i TIC, Escola Tècnica Superior d'Enginyeria de Mines de Manresa, Universitat Politècnica de Catalunya, Avinguda de les Bases de Manresa 61–73, 08242 Manresa, Spain; elidaccf@gmail.com (E.C.); arnau.martinez.alcala@upc.edu (A.M.); maria.teresa.yubero@upc.edu (M.T.Y.); hernan.anticoi@upc.edu (H.A.)

[2] Departament de Mineralogia, Petrologia i Prospecció Geològica, Facultat de Ciències de la Terra, Universitat de Barcelona, Carrer de Martí i Franquès s/n, 08028 Barcelona, Spain; maitegarciavalles@ub.edu

* Correspondence: maria.pura.alfonso@upc.edu; Tel.: +34-938777292

Abstract: A mineralogical and mineral chemistry study was carried out in the San Luis Alta telluride-rich gold deposit, mid-south Peru, to contribute towards determining its formation and improving the ore processing. The San Luis mineralization is considered an intrusion-related gold deposit located in the Arequipa segment of the Coastal Batholith. The mineralization occurs in quartz veins hosted in diorites and granodiorites from the Tiabaya Super-Unit. These veins are sulfide-rich in the deep areas and contain abundant iron oxides. Sulfides are mainly pyrite with minor chalcopyrite and galena. Native gold and telluride minerals are abundant. Mineral chemistry was determined using an electron microprobe. The mineralogy of veins was classified into four stages. Gold occurs in the three last stages either in large grains, visible to the naked eye, or, more frequently, in grains of less than 10 µm. Gold appears as grains encapsulated in pyrite, Fe oxides, quartz and filling fractures. The first stage is characterized by the deposition of quartz and massive pyrite, which does not contain gold. During the second stage, hessite, calaverite, petzite and altaite are formed. Additionally, Bi-tellurides, mainly volynskite, rucklidgeite, kochkarite and tellurobusmuthine, are formed. Some of these minerals occur as blebs encapsulated in pyrite, suggesting that a Bi-Te-rich melt was formed from the ore-forming hydrothermal fluid and transported the Au and Ag elements. This stage was followed by a fracturing event and tellurobismuthite, tetradymite and montbrayite precipitated. In the last stage, a supergene replacement formed covellite, bornite and goethite. Te-Bi minerals do not appear in this stage, but selenium minerals occur in minor amounts. Chlorargyrite and iodargyrite occur and are associated with gold.

Keywords: gold; tellurides; intrusion-related gold deposits; Peru

Citation: Alfonso, P.; Ccolqque, E.; Garcia-Valles, M.; Martínez, A.; Yubero, M.T.; Anticoi, H.; Sidki-Rius, N. Mineralogy and Mineral Chemistry of the Au-Ag-Te-(Bi-Se) San Luis Alta Deposit, Mid-South Peru. *Minerals* **2023**, *13*, 568. https://doi.org/10.3390/min13040568

Academic Editor: Stefano Salvi

Received: 31 March 2023
Revised: 14 April 2023
Accepted: 17 April 2023
Published: 18 April 2023

1. Introduction

The occurrence of tellurides, and, to a lesser extent, selenides, is frequent in some gold deposits. The study of these associations is important both for establishing the formation conditions of the deposits and also for the implications that such mineralogy has for further processing the ores. Telluride minerals provide information on the physicochemical conditions of the deposits formation, including temperature, O_2, S, Te, Bi fugacity and pH, among others [1–4]. The presence of high Te and Bi contents influences the behavior of gold during the formation of the deposits. The high Te and Bi contents act on the hydrothermal fluids that transport them and favor the fractionation of melts that scavenge gold, which is deposited in association with Te and Bi minerals [1,2,5,6]. Therefore, the determination of the mineralogy will be fundamental to the establishment of the deposit model.

On the other hand, gold associated with tellurides is part of the so-called refractory gold. A detailed knowledge of the mineralogy of the gold ores is necessary and must be

considered in formulating the most appropriate processing system for gold recovery [7–9]. The most common method used for gold recovery is cyanidation, but ores containing tellurides must undergo an oxidation pre-treatment before immersion in the cyanide solution. Additionally, during chemical analysis, the presence of tellurides can lead to an underestimation of the gold content [10].

Although Te-Au-Ag-Bi associations have been described more frequently in epithermal deposits, they have also been reported in several intrusion-related gold deposits such as the Salave deposit in northern Spain [11,12], the Golden Mile deposit in Australia [13], the Deer Horn deposit in British Columbia [14] and several deposits in north-east Russia [15,16].

In the mid-south region of Peru, more than 70 deposits are located in the Nazca-Palpa Ocoña belt [17]. Most of them are currently exploited by artisanal mining, including San Luis Alta, Filomena, Santa Rosa, Estrella, Posco-Misky, Calpa, Ishihuinca, Sol de Oro, Los Incas, San Juan de Chorunga, and Mollehuaca [18]. However, they have been poorly studied. Based on regional studies, they have been classified into the intrusion-related gold type [19,20], although, in other cases, they were classified into the orogenic gold type [21,22]. Recently, the study area has benefited from the publication of two articles that represent the first contributions on the mineralogy of deposits from the Nazca-Palpa-Ocoña belt [9,23]. The first one provides a general review of the mineralogy of five deposits in the area, including the San Luis Alta and Santa Filomena deposits. The second one, by Crespo et al. [23], is mainly focused on the Mollehuaca and San Juan de Chorunga deposits.

This work presents a detailed study of the mineralogy and mineral chemistry of the San Luis Alta deposit and compares it with some of those found in the same belt in order to obtain characteristics of its formation that will help us carry out more in-depth genetic studies in the future. Another benefit associated with the detailed knowledge of the deposit mineralogy is the contribution to the improvement in the planning of the processing of these ores for the optimal recovery of gold.

2. Geological Setting

The San Luis Alta deposit is located in the southern part of the Nazca-Palpa-Ocoña belt. This belt extends over 350 km along the coast of Peru, which extends more than 350 km along the southern Coastal Batholith. This batholith is constituted by numerous Mesozoic plutonic bodies and crops out almost continuously along the Western Cordillera of Peru, extending more than 1600 km parallel to the coast and is more than 65 km wide [24]. The batholith is divided into two segments, the segment of Lima, with 11 units and the Arequipa segment, with 5 units: Patap, Linga, Pampahuasi, Incahuasi and Tiabaya. The Patap Superunit is made up of gabbro; the Linga Superunit is composed of rocks between monzodiorite and monzogranite; the Pampahuasi Superunit is composed of tonalities; the Incahuasi Superunit represents the largest volume of the batholith and is comprised of large plutons consisting mainly of monzodiorites. Finally, the Tiabaya Superunit is the youngest and most important of the five, as it outcrops along the entire Arequipa segment, showing cross-sectional relationships with all previous intrusions. The lithology varies from diorites to monzogranites, with granodiorites being the most abundant rocks. Their age is between 102 and 80 Ma [24], or more narrowly defined, between 76 and 79 Ma [25].

From the metallogenic point of view, Peru is divided into 23 belts: 12 of them are gold belts, and the studied area belongs to belt IX, corresponding to Au-Pb-Zn-Cu intrusion-related deposits of the Upper Cretaceous age. This belt is divided into three areas; one of them is the Nazca-Palpa-Ocoña [19,26], which, in turn, belongs to the Arequipa segment.

The San Luis Alta deposit is hosted in the Tiabaya superunit (Figure 1). This superunit is mainly made up of granodiorites and diorites with the typical mineralogy of K-feldspar, plagioclase, biotite, hornblende and a variable amount of quartz. In San Luis, some alignment of hornblende and biotite crystals is often observed, causing a slight foliation in the rock. In addition, 1.5 m thick andesitic dykes with a N320° orientation and dipping 70° to the northeast cross-cut granodiorite and E–W veins.

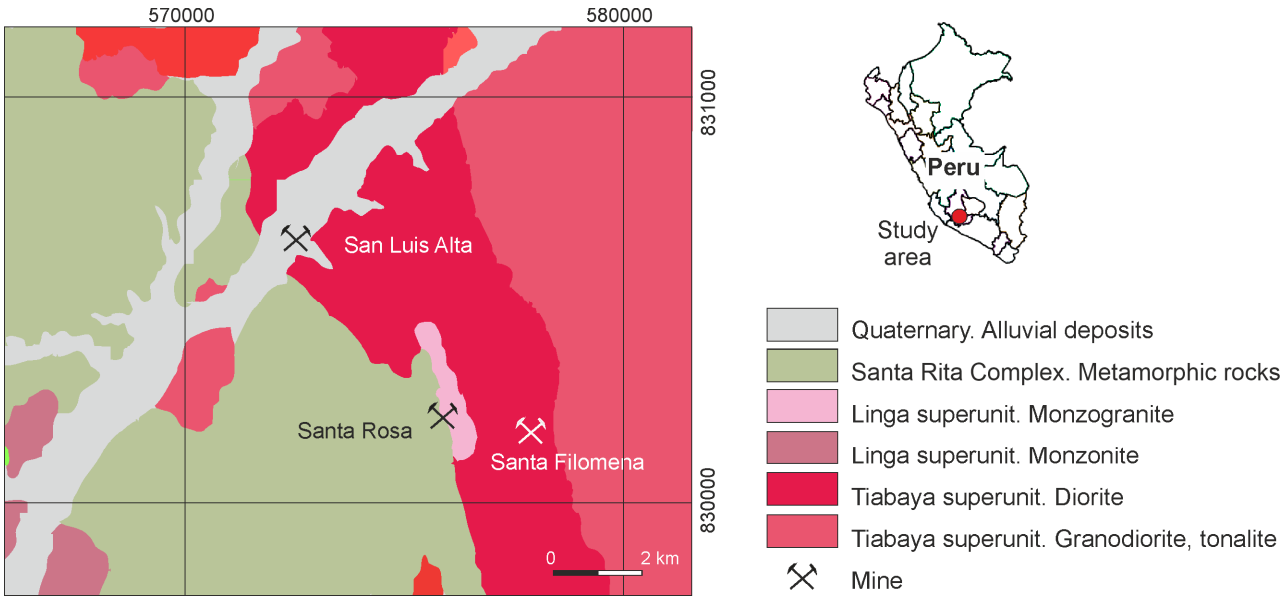

Figure 1. Geological map of the San Luis Alta and Filomena deposits.

At the western contact of the San Luis deposit, the Santa Rita Complex outcrops. This consists of pyroxenic diorites and andesites affected by contact metamorphism due to the intrusion of the Linga and Tiabaya superunits. On the surface, the San Luis deposit is covered by Quaternary alluvial and colluvial deposits.

At San Luis Alta, the gold mineralization occurs in fault-controlled quartz veins mainly hosted in diorites and granodiorites. The veins occur as the filling of spaces left by the formation of faults, frequently trending in the NW–SE and E–W directions. NW–SE-trending veins are the longest; they are usually less than 1 m thick, in the N310° direction, dipping from 70° NE to nearly vertical. W–E-trending veins are in the N270° direction, dip around 45–60° and are younger. The veins can be observed in the mine shafts, but they never outcrop at the surface. The veins are filled by quartz that often is brecciated and contains abundant fractures filled with Fe-oxides. In some areas, they are especially rich in minerals with copper, with alterations of malachite and minor azurite. In other cases, sulfide-rich mineralization accompanies quartz. The most abundant sulfide is pyrite. Its content is moderate but increases with depth, becoming massive below 600 m.

In this deposit, the main vein is the so-called San Luis vein (Figure 2), with a N50W direction and a 45° NE dip, being up to 1.5 m in thickness and outcropping over 800 m. The other important veins are the Clider, Ramal, Débora and Carolina.

In the contact of the veins with the host rock, there is marked hydrothermal alteration, with moderate-to-weak silicification and subordinate phyllic and argillic alteration, with the formation of sericite, kaolinite and, occasionally, epidote.

The area has undergone a stage of supergene alteration with an upper part, or oxidation zone, about 80 m thick, with hematite, goethite, chrysocolla, malachite, atacamite, cuprite, malachite and the secondary enrichment zone, about 100 m thick, with gold mineralization, native silver, chlorargyrite, iodargyrite, covellite and bornite. Mining is carried out in both the secondary and hypogene zones, where pyrite occurs associated with quartz.

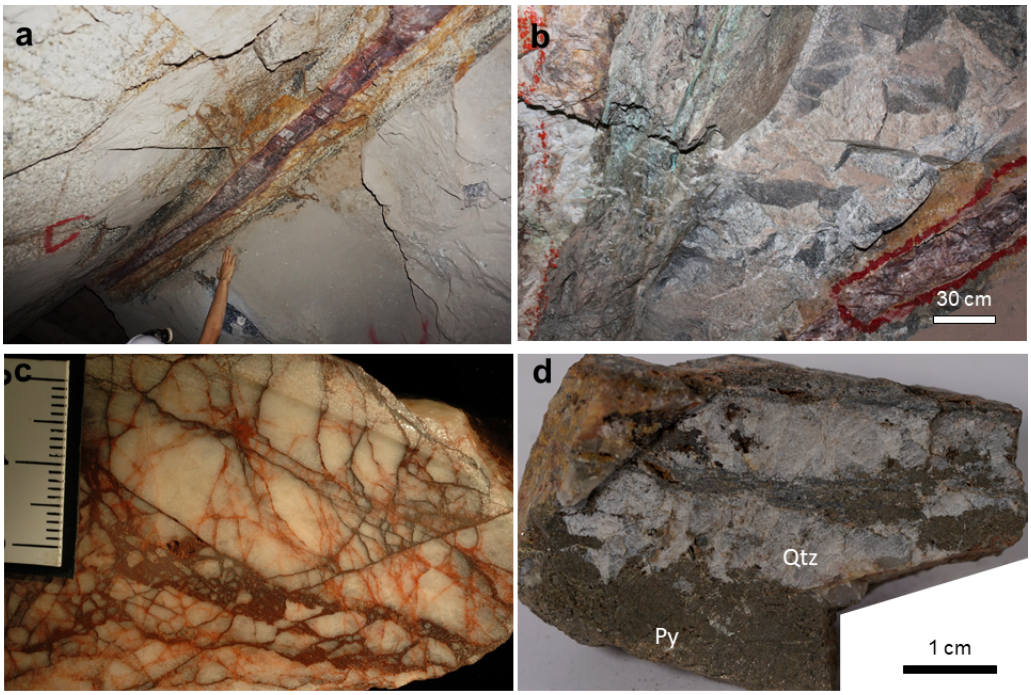

Figure 2. Images of the San Luis vein: (**a**) general view; (**b**) yhe presence of malachite and chrysocolla is locally abundant; (**c**) detail of a sample from this vein, where quartz (Qtz) and iron oxides with a brecciated structure are observed; (**d**) the vein in the deep parts of the mine, where pyrite (Py) occurs in massive beds.

The Filomena deposit, located about 5 km from the San Luis Alta deposit, is also hosted in the Tiabaya superunit. This deposit consists of veins with a mainly WNW–WSE direction, up to 25 cm thick and more than 1000 m long. Their mineralogy also consists mainly of quartz, with an abundance of Fe oxides.

The gold grade of the San Luis Alta veins usually is between 40 and 60 g/t, but locally, it reaches up to 121 g/t, and the Te content varies between less than 10 and up to 180 g/t. The Filomena deposit has negligible Te contents [9].

3. Materials and Methods

A total of 21 mine shaft samples were obtained from the San Luis deposit. Samples were taken at different points up to 400 m in depth. The Santa Filomena deposit was also sampled. The samples were studied in thin and thick polished sections by transmitted and reflected light optical microscopy, X-ray diffraction (XRD), scanning electron microscopy with energy-dispersive analyzer (SEM-EDS) and electron probe microanalysis (EPMA).

The XRD equipment was a PANalytical XPert PRO MPD alpha1 diffractometer with a focalized primary monochromator and an Xcelerator detector located at the Centres Cientifics i Tecnològics de la Universitat de Barcelona (CCiT-UB). The radiation used was $K\alpha_1$ Cu (λ = 1.5406 Å) at 45 kV and 40 mA. The spectra were interpreted using the PANalytical XPert HighScore software.

The SEM-EDS equipment used were a Hitachi TM-100 and an ESEM Quanta 200 FEI XTE 325/D8395 electron microscope with an INCA Energy 250 EDS detector attached. The latter operated at 20–25 keV, 1 nA and at a working distance of 10 mm.

The mineral chemistry of gold-bearing minerals and pyrite was quantitatively determined using a CAMECA SX–50 and JEOL JXA-8230 electron microprobe at the CCiT-UB. The conditions of analysis were 25 kV and 20 nA, with a beam diameter of 1–5 µm and a counting time of 10 s. Natural and synthetic standards were used for external calibration.

4. Results

4.1. Mineralogy

The veins of San Luis Alta are filled with milky quartz and minor contents of sericite, chlorite and calcite, the latter with a mean content of 3 wt.%. The sulfide and oxide mineralogy has different characteristics depending on whether they are in the superficial or more internal part, with predominantly sulfides at depth and oxides at the surface level. Veins were hydrothermally brecciated, and fractures were filled with iron oxides.

4.1.1. Sulfides

At least two generations of pyrite can be distinguished. The first generation crystallizes as massive, hosted in quartz, with no inclusion of other minerals. A later generation differs from the previous one by having a large number of mineral inclusions of gold, tellurides, galena and chalcopyrite. This pyrite is usually crossed by fractures in which iron oxides appear. In both generations, pyrite occurs as anhedral grains.

Galena, chalcopyrite, covellite and bornite occur in minor amounts, usually as inclusions in pyrite.

4.1.2. Native Gold

Native gold is found in different morphologies and it has precipitated at different stages (Figure 3). The first generation is found in isolated grains encapsulated in pyrite and also in quartz, where it forms surrounded grains. It also occurs within hematite. A second generation is found filling fractures or voids. In other deposits of the Nazca-Palpa-Ocoña belt, the gold that occurs filling fractures is of the electrum type [9]. A late gold generation is found associated with iron oxides. In this case, gold often has a fibrous morphology (Figure 3g–k) or a porous aspect (Figure 3l). This morphology was also reported by Zhao et al. [27] for gold replacing calaverite. Gold often occurs as a rim of a telluride association.

The chemical composition of gold grains (Table 1) varies according to the physicochemical conditions of formation. Gold can form a solid solution with Ag and minor amounts of Cu. The gold grains in San Luis Alta range from 82 to 97.8 wt.%, while the Ag content is between 13.74 and 2.0 wt.%, and Cu content can reach up to 0.18 wt.%. Therefore, electrum is never present if it is understood in the usual way, where this name is applied when the Ag contents represent more than 20 wt.% [28].

Table 1. Electron microprobe analyses (wt.%) of native gold from the San Luis deposit (SL) and the close Santa Filomena deposit (F). Au, Ag and Cu are calculated on the basis of one a.p.f.u. (atoms per formula unit).

Element	F28-06	F28-08	SL21-01	SL21-07	SL21-21	SL107-21	SL13-07	SL13-08	SL107-17	SL103-52	SL103-70
Au	94.63	86.58	90.45	88.65	82.28	84.03	90.58	92.77	89.69	83.93	97.82
Ag	4.00	12.70	9.74	10.88	15.53	13.34	7.13	6.38	9.13	10.28	3.36
Cu	0.05	0.00	0.00	0.08	0.17	0.18	0.03	0.02	0.00	0.03	0.10
S	0.08	0.14	0.04	0.04	0.32	n.a.	0.17	0.06	n.a.	n.a.	n.a.
Fe	0.36	0.02	0.33	0.49	2.18	1.54	2.35	0.81	0.26	4.62	0.36
As	0.00	0.01	0.00	0.00	0.00	n.a.	0.04	0.22	n.a.	n.a.	n.a.
Se	0.00	0.12	0.00	0.00	0.11	0.18	0.06	0.06	0.15	0.13	0.05
Sb	0.00	0.01	0.01	0.00	0.02	0.01	0.00	0.03	0.00	0.03	0.00
Bi	0.07	0.00	0.00	0.00	0.00	0.71	0.07	0.01	0.73	0.75	0.85
Sum	99.18	99.58	100.56	100.14	100.61	99.99	100.43	100.36	99.97	99.78	102.54
A.p.f.u											
Au	0.93	0.79	0.84	0.82	0.74	0.77	0.87	0.89	0.84	0.82	0.94
Ag	0.07	0.21	0.16	0.18	0.26	0.22	0.13	0.11	0.16	0.18	0.06
Cu	0.00	0.00	0.00	0.00	0.00	0.01	0.00	0.00	0.00	0.00	0.00

n.a.: not analyzed.

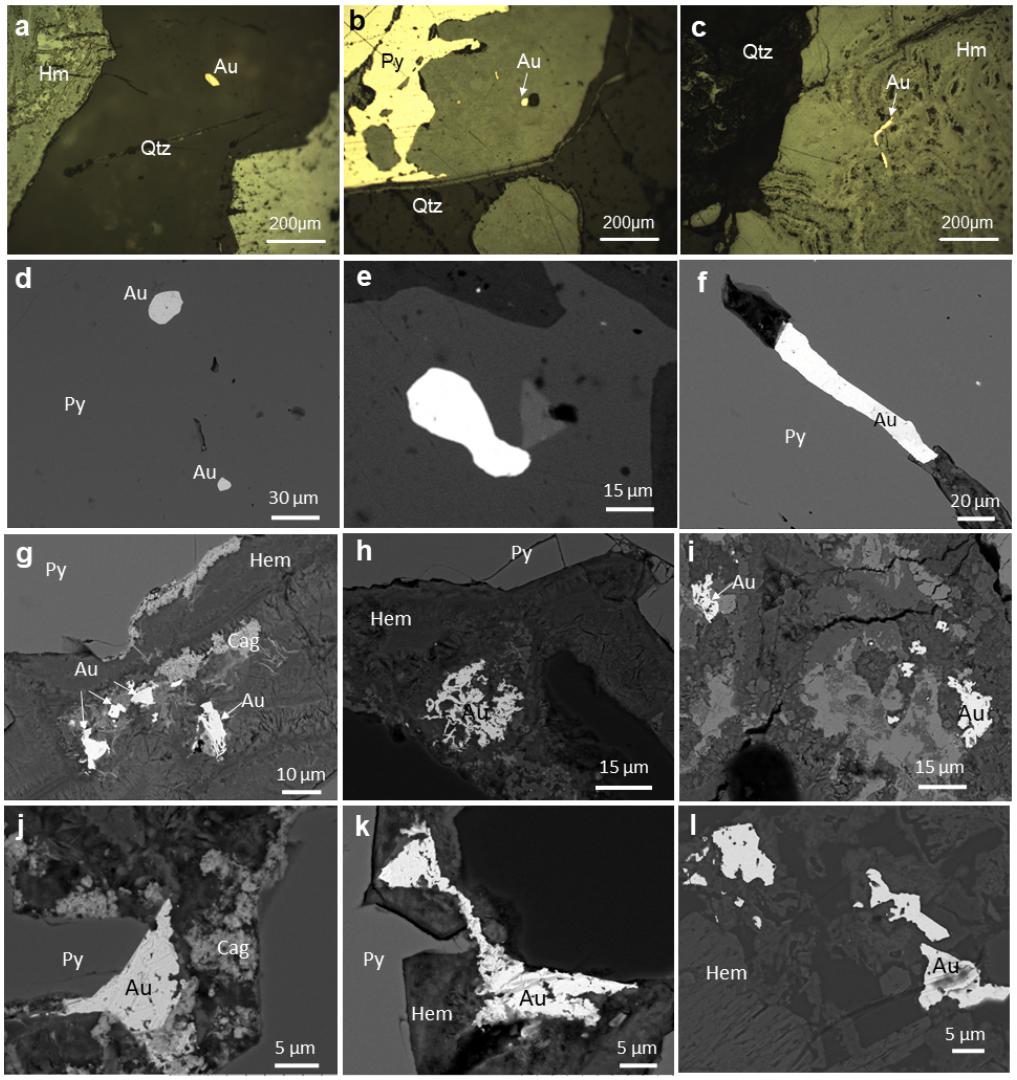

Figure 3. Reflected light photomicrographs (**a**–**c**) and SEM images (**d**–**l**) of gold from the San Luis Alta deposit: (**a**) gold grain enclosed in quartz; (**b**) gold hosted in hematite (Hm); (**c**) gold filament in hematite; (**d**,**e**) isolated rounded gold grains in pyrite; (**f**) gold filling fractures in pyrite; (**g**) thin filaments of late gold on chlorargyrite (Cag); (**h**) filamentous gold in hematite; (**i**) late gold filaments next to alteration minerals; (**j**) gold associated with chlorargyrite; (**k**) late gold on hematite; (**l**) porous gold. Images (**g**–**l**) belong to a supergene stage.

The Fe content can reach high values, usually up to 2.5 wt.%, and occasionally even over 4 wt.%. These contents are probably due to the presence of Fe oxide inclusions, giving rise to the so-called mustard gold. This type of gold is common in telluride gold deposits [27,29,30]. The formation of this type of gold was attributed to the selective leaching of Te from gold tellurides during alteration [27,31]. Similar to what happens in the Oleninskoe deposit [32], mustard gold usually occurs associated with chlorargyrite (Figure 3i–k).

Townley et al. [33] reported a ternary diagram to define the contents in Ag and Cu according to different deposit types. In Figure 4, the San Luis Alta and other intrusion-related gold deposits from mid-south Peru are plotted [8]. The proportions of Au, Ag and Cu show scattered values, with richer Cu contents in the Cháparra deposit. In the case of San Luis, the values are similar to those indicated for the Au-rich porphyry deposits.

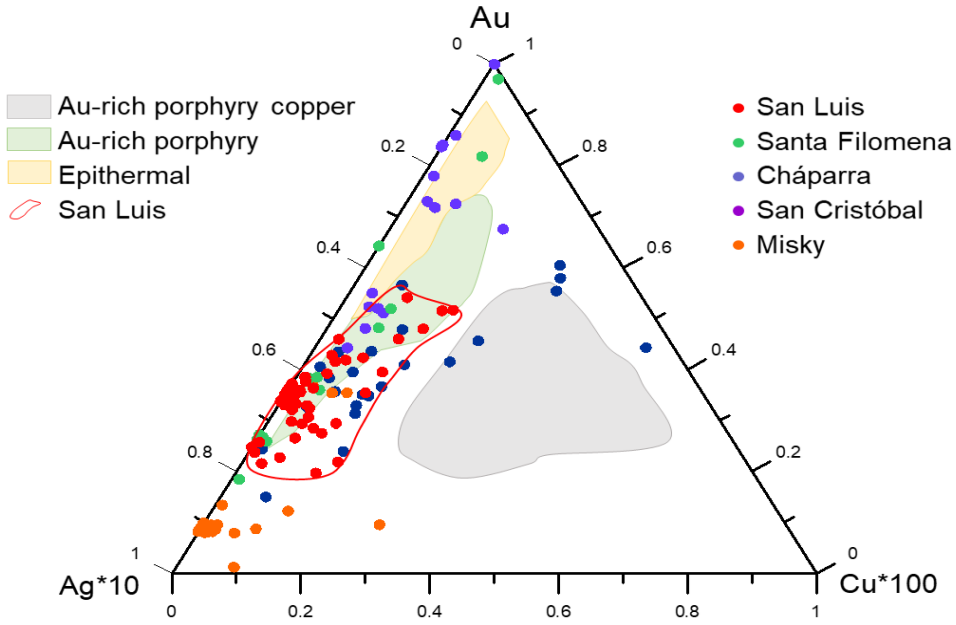

Figure 4. Au–(Ag*10)–(Cu*100) compositional diagram, atomic %, of several intrusion-related gold deposits from mid-south Peru. Comparison with compositional fields established for epithermal, Au-rich porphyry Cu and Au-rich porphyry deposits [33].

4.1.3. Au, Ag Tellurides

Tellurides from San Luis Alta occur as grains of a few µm in size, usually associated with each other and with gold (Figure 5). The Au and Ag tellurides are mainly calaverite, petzite and hessite. Sylvanite and altaite are scarce. All these phases are found in grains within pyrite or as void fillers. They also coexist with galena and chalcopyrite in sharp contacts (Figure 5b,d). They can coexist or be partially replaced by Bi telluride minerals such as volynskite, rucklidgeite and kochkarite (Figure 5d–l).

The chemical composition of representative samples is shown in Table 2. The chemical composition of calaverite is close to the ideal formula, containing up to 0.91 wt.% Ag. Petzite contains 21.50–25.41 wt.% Au, 35.70–41.57 wt.% Ag and 30.90–33.78 wt.% Te. Hessite contains up to 0.89 wt.% Au, 60.93–61.89 wt.% Ag and 37.74–38.64 wt.% Te. Grains with compositions between calaverite and petzite and between petzite and hessite, with nearly stoichiometric proportions, have been determined and correspond to a formula of $Ag_{2.02}Au_{0.99}Te_{1.99}$ and $(Ag_{2.03}Au_{0.98})Te_{1.98}$, respectively. Intermediate compositions between these minerals are possible, as they even form continuous solid solutions at high temperatures [34]. These solid solutions breakdown at low temperatures and exsolution textures of hessite and petzite can be developed [35].

Table 2. Representative EPMA analyses and calculated formulae (a.p.f.u) of Au, Ag and Pb tellurides from San Luis Alta.

Mineral	Clv	Clv	Ptz	Ptz	Ptz	$AuAg_2Te_2$	Ag_2AuTe_2	Hes	Hes	Hes
Sample	**L13-04**	**L21-97**	**L21-93**	**L103-3**	**L21-87**	**L103-44**	**L103-46**	**L103-4**	**L21-13**	**L21-91**
Au	41.39	41.43	25.21	21.46	24.83	28.22	28.98	7.50	0.03	0.00
Ag	0.74	0.91	40.82	41.17	40.07	32.02	32.31	52.72	61.89	60.93
Sb	0.39	0.43	0.28	0.17	0.22	0.29	0.23	0.21	0.26	0.24
Te	57.13	56.86	31.35	33.23	33.72	36.91	37.70	33.21	38.32	38.03
Se	0.00	0.00	0.11	0.06	0.10	0.18	0.13	0.12	0.00	0.01
S	0.08	0.14	0.14	0.83	0.26	0.39	0.56	0.92	0.10	0.09
Cu	0.07	0.08	0.00	0.01	0.01	0.00	0.02	0.07	0.05	0.02
Fe	0.99	1.32	0.68	2.30	1.42	2.55	0.50	2.66	0.56	-
Pb	-	-	-	0.09	0.10	-	-	0.27	-	0.70
Bi	0.43	0.35	0.23	0.23	0.22	0.29	0.32	0.09	0.02	-
Total	101.22	101.52	98.82	99.54	100.95	100.85	100.74	97.77	101.23	100.02

Table 2. *Cont.*

Mineral	Clv	Clv	Ptz	Ptz	Ptz	$AuAg_2Te_2$	Ag_2AuTe_2	Hes	Hes	Hes
Sample	**L13-04**	**L21-97**	**L21-93**	**L103-3**	**L21-87**	**L103-44**	**L103-46**	**L103-4**	**L21-13**	**L21-91**
a.p.f.u	3	3	6	6	6	5	5	3	3	3
Au	0.944	0.945	1.009	0.837	0.976	0.958	0.962	0.139	0.001	-
Ag	0.031	0.038	2.982	2.933	2.877	1.985	1.958	1.784	1.955	1.945
Sb	0.014	0.016	0.018	0.011	0.014	0.016	0.012	0.006	0.007	0.007
Te	2.011	2.001	1.936	2.001	2.047	1.934	1.932	0.950	1.023	1.026
Se	0.000	0.000	0.011	0.006	0.010	0.015	0.011	0.006	0.000	0.000
S	0.011	0.019	0.035	0.198	0.063	0.082	0.113	0.105	0.010	0.010
Cu	0.005	0.006	0.000	0.001	0.001	0.000	0.002	0.004	0.003	0.001
Pb	-	0.000	-	0.003	0.004	-	-	0.005	-	0.012
Bi	0.009	0.008	0.008	0.008	0.008	0.009	0.010	0.001	-	-

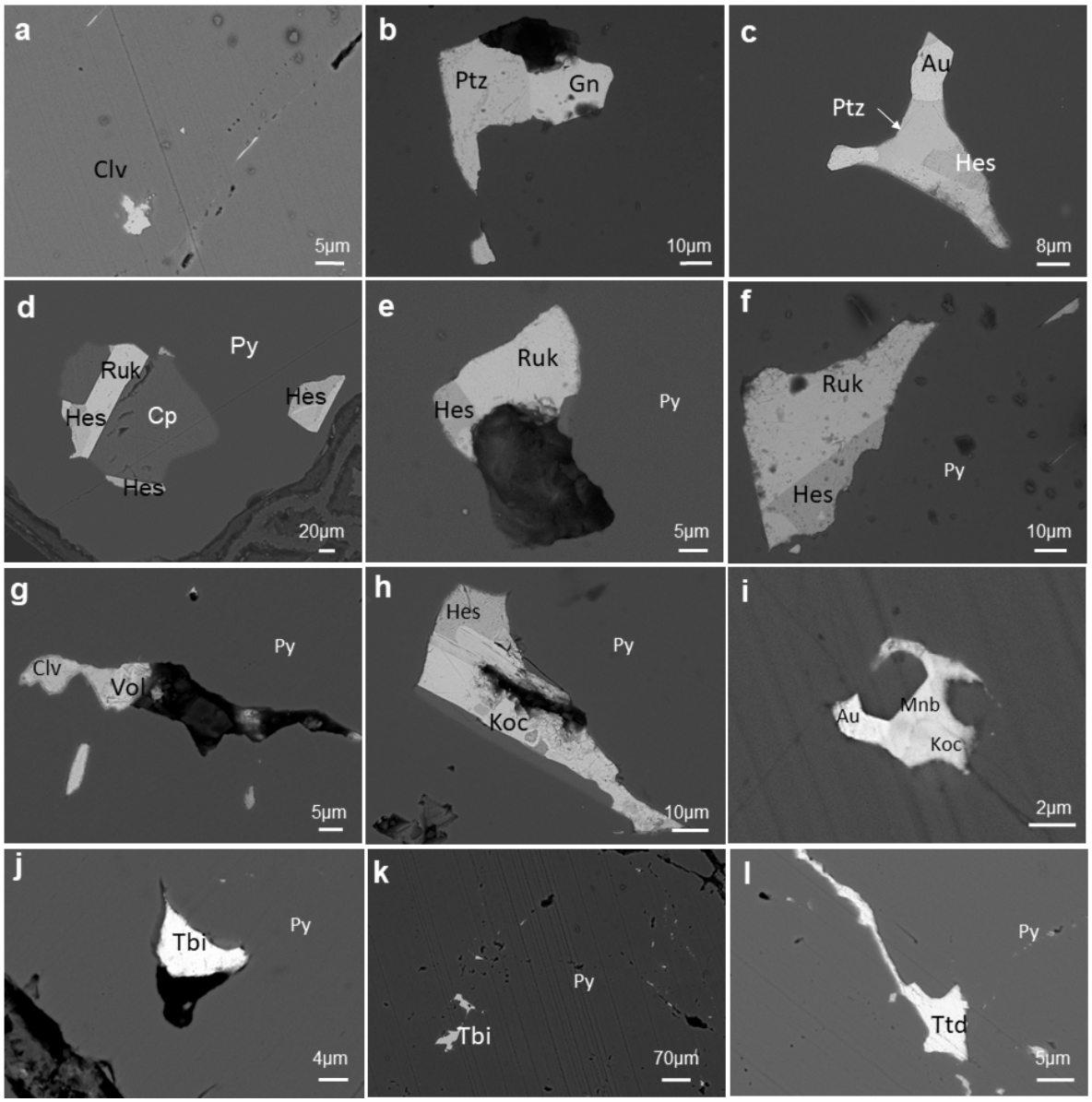

Figure 5. SEM images of Au-Ag-Te-Bi association from the San Luis deposit: (**a**) calaverite (Clv); (**b**) petzite (Ptz) coexisting with galena (Gn), showing a sharp contact; (**c**) hessite (Hes) is replaced by petzite (Ptz) and this is followed by a late generation of gold; (**d**) inclusion of hessite and rucklidgeite (Ruk) in chalcopyrite (Cp), in turn included in pyrite; (**e**,**f**) hessite coexisting with rucklidgeite; (**g**) calaverite coexisting with volynskite (Vol); (**h**) hessite replaced by Kochkarite (Koc); (**i**) kochkarite replaced by montbrayite (Mnb) and a coexisting with gold; (**j**–**l**) tellurobismuthite and tetradymite (Ttd) filling voids and fractures.

4.1.4. Bi Tellurides

Bi tellurides occur associated with Au tellurides and with gold. Montbrayite is the only Au-rich Bi telluride and has the complex formula: $(Au,Ag,Sb,Bi,Pb)_{23}(TeSb,Bi,Pb)_{38}$. The most abundant Bi telluride is tellurobismuthite. Volynskite, kochkarite, rucklidgeite and tetradymite were also identified by EPMA (Table 3). Tellurobismuthite has up to 1.68 wt.% of S and up to 0.34 wt.% Sb, which is justified by the extensive solid-solution between tellurobismuthite and bismuthite [36].

Table 3. Representative EPMA analyses and calculated formulae of Bi tellurides and selenides from San Luis Alta.

Mineral	Tbi	Tbi	Ttd	Vol	Vol	Ruk	Ruk	Koc	Koc	Mnb	Fis
Sample	**L103-28**	**L21-99**	**R1-10**	**L21-114**	**L21-83**		**L21-84**	**L21-89**	**L21-90**	**L21-03**	**L103-42**
Au	0.00	0.00	0.02	0.00	1.08	0.00	0.00	0.00	0.00	26.55	26.86
Ag	0.00	0.12	0.03	18.75	14.75	1.23	4.69	0.77	2.53	0.86	47.20
Sb	0.33	0.42	0.18	0.27	0.30	0.27	0.34	0.32	0.33	0.27	0.00
Te	46.87	47.39	35.60	43.96	43.93	45.96	42.55	44.47	45.61	44.94	0.12
Se	0.14	0.14	0.16	0.26	0.26	0.14	0.10	0.22	0.21	0.07	24.05
S	0.28	0.10	4.31	0.06	0.43	0.07	0.12	0.30	0.13	1.32	0.10
Cu	0.00	0.02	0.03	0.00	0.01	0.00	0.02	0.02	0.02	0.09	0.04
Fe	2.24	1.36	1.65	0.88	2.62	0.31	1.28	1.76	1.05	3.22	0.65
Pb	0.00	0.08	0.00	0.09	3.68	12.33	11.18	9.46	9.68	0.13	0.09
Bi	50.39	51.07	56.94	35.76	33.16	40.46	39.40	40.88	42.25	20.73	0.22
Total	100.25	100.69	98.92	100.03	100.22	100.77	99.68	98.19	101.81	98.17	104.33
a.p.f.u	5	5	5	4	4	7	7	12	12	61	6
Au	0.000	0.000	0.001	0.000	0.032	0.000	0.000	0.000	0.000	12.840	0.913
Ag	0.000	0.009	0.002	0.997	0.802	0.127	0.485	0.139	0.440	0.756	2.929
Sb	0.021	0.027	0.010	0.013	0.015	0.024	0.031	0.051	0.051	0.210	0.000
Te	2.954	2.967	2.021	1.976	2.019	3.997	3.720	6.834	6.707	33.549	0.006
Se	0.014	0.014	0.015	0.019	0.019	0.020	0.015	0.054	0.049	0.083	2.039
S	0.070	0.025	0.974	0.012	0.078	0.023	0.040	0.186	0.076	3.921	0.021
Cu	0.000	0.002	0.004	0.000	0.001	0.000	0.003	0.005	0.007	0.131	0.004
Pb	0.000	0.003	0.000	0.002	0.104	0.660	0.602	0.895	0.877	0.061	0.003
Bi	1.939	1.952	1.974	0.982	0.931	2.148	2.103	3.836	3.794	9.449	0.007

Tetradymite also occurs in minor amounts as inclusions of elongated to rounded grains and filling fractures in pyrite. Bi and Te occur associated with Ag as volynskite.

Volynskite contains between 14.75 and 18.75 wt.% Ag and the Cu content is low, up to 0.01 wt.% Cu, and up to 0.26 wt.% Se. The Pb-bearing Bi tellurides are kochkarite and rucklidgeite. Kochkarite contains between 8.39 and 11.18 wt.% Pb and up to 4.69 wt.% Ag, whereas rucklidgeite contains from 12.31 to 15.24 wt.% Pb and up to 1.72 wt.% Ag. These high Ag contents may be due to the close distribution with hessite and petzite. Ag-Pb-Bi-Sb-Te minerals often form solid solutions [37], as can be observed in Figure 6 between rucklidgeite and kochkarite. The compositional map in Figure 7 shows that Te forms discrete phases, while Bi appears in more diffuse contacts with other tellurides. In Figure 7b, the exsolution textures of hessite in volynskite can be observed.

4.1.5. Selenides

The only selenide minerals observed are fischesserite and a Cu, Hg selenide regarding which EDS analyses provide a formula close to brodtkorbite (Figure 8). Fischesserite occurs as crystals a few μm across as a late phase included in the innermost part of the iron oxide veinlets that crosscut pyrite. Fischesserite can contain up to 0.40 wt.% Te, 0.03 wt.% Sb and 0.35 wt.% Bi (Table 3). This mineral is rare but was also found in the Kupol epithermal deposit, Russia [38], in Ulug-Sair, Russia [39], and in Rincón Blanco, Argentina [40].

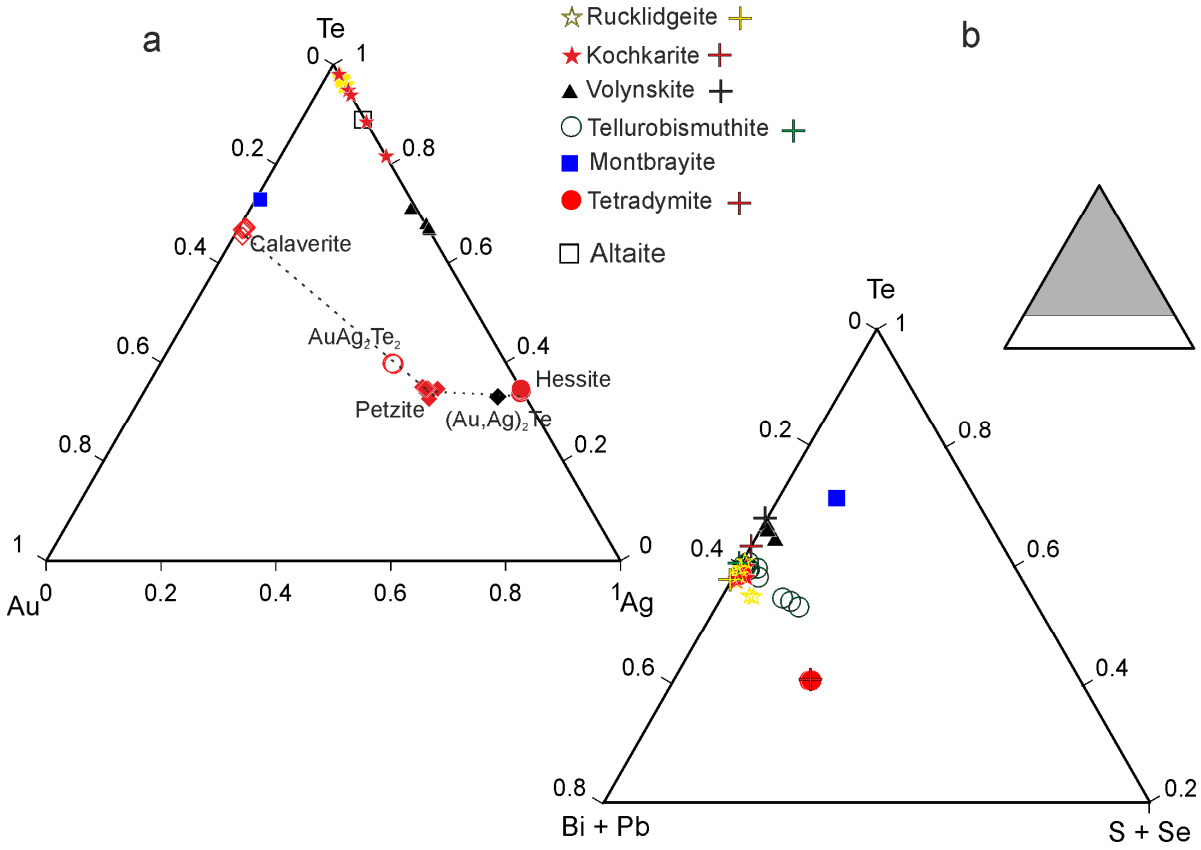

Figure 6. Triangular plots, atomic %, of tellurides from San Luis Alta: (**a**) Te-Au-Ag; (**b**) Te-Bi+Pb-S+Se.

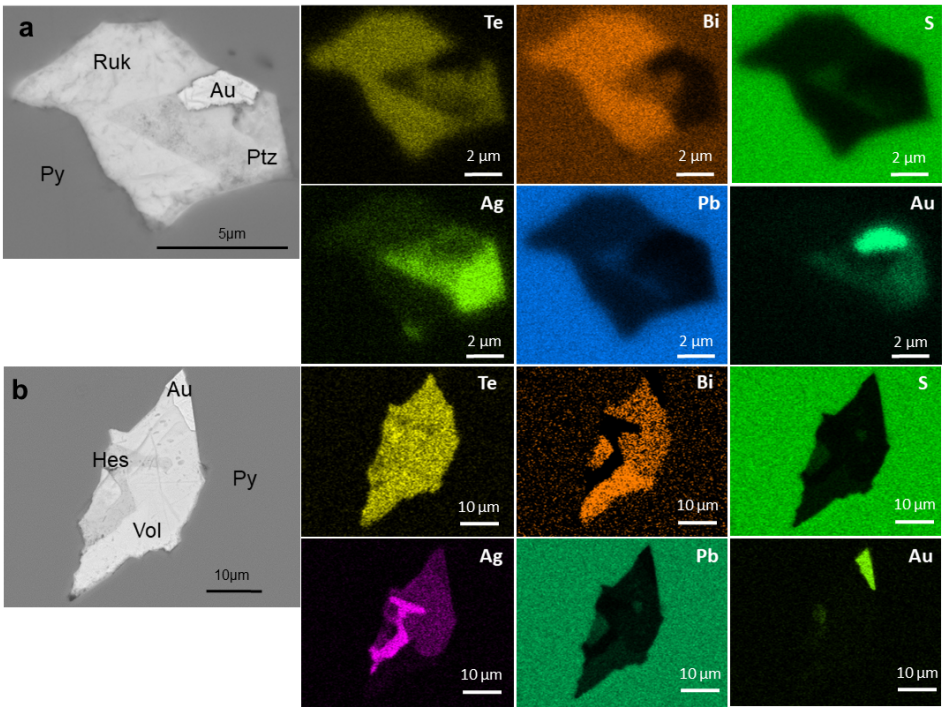

Figure 7. SEM-EDS compositional mapping of an Au-Ag-Te-Bi-Pb bleb for Te, Bi, S, Ag, Pb and Au: (**a**) rucklidgeite–petzite association; (**b**) hessite–volynskite association. Note the small blebs of hessite in volynskite.

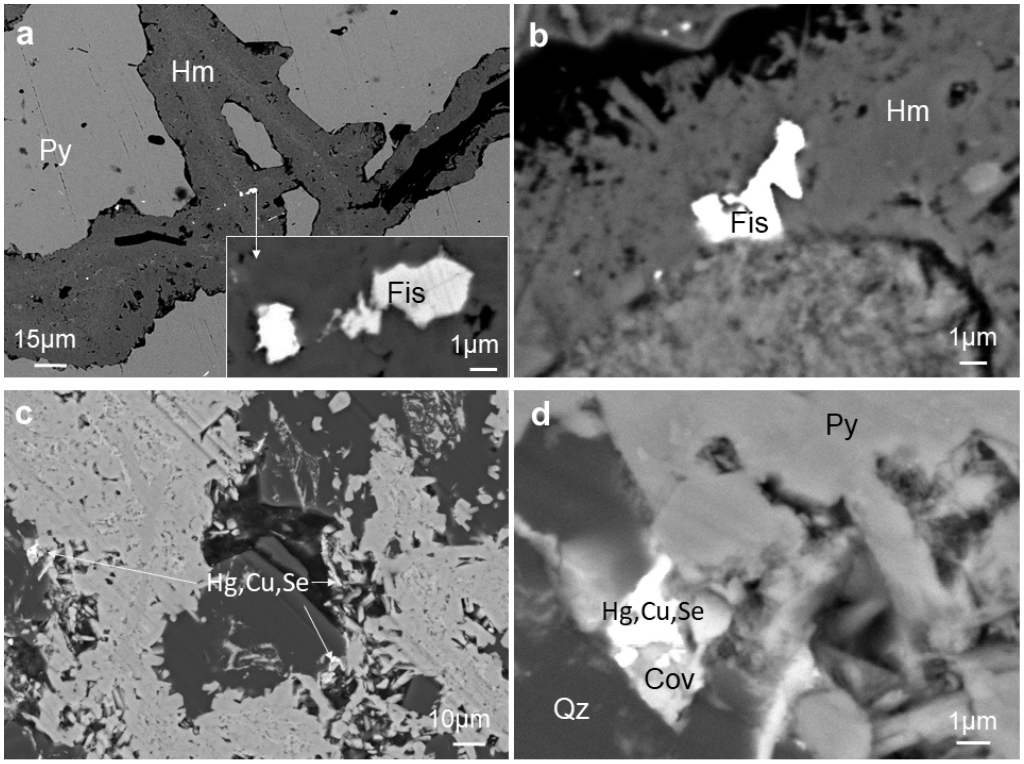

Figure 8. SEM images of selenides from the San Luis deposit: (**a**,**b**) fischesserite hosted in hematite; (**c**) brodtkorbite is located along the boundary of hematite and quartz; (**d**) detail of the selenide shown in the left side of image (**c**).

Brodtkorbite is the only Hg-rich mineral found in San Luis. As in other cases [41], it contains small amounts of Ag in addition to Hg, Cu and Se. This mineral occurs only in the Débora vein and is mainly found at the boundary of iron oxides and quartz associated with covellite.

4.2. Paragenetic Sequence

A paragenetic sequence based on four stages has been reconstructed on the basis of the textural relationships among the various minerals present in the San Luis Alta gold veins: Stage I, or primary mineralization, a second stage of fracture and fracture modification, a third stage of oxidation and a last stage of supergene alteration (Figure 9).

The sequence begins with the development of fractures, some of them at regional scale, which are filled with milky quartz. The circulation of hydrothermal fluids produces the precipitation of a first generation of pyrite. Native gold occurs from this early event as inclusions within the pyrite in regular morphology grains (Figure 3d,e).

In the second stage, in addition to pyrite precipitation, smaller amounts of other sulfides precipitate, mainly galena and chalcopyrite. In association with these, tellurides and some Bi-Te minerals appear. The first telluride to precipitate is hessite. The same is observed in other deposits such as the Fancha deposit in China, which was attributed to the fact that this mineral requires a lower fugacity of Te for its formation [42]. Calaverite and petzite also precipitate at this time, whereas, in reduced deposits, such as Misky, silver occurs as an electrum, rather than as a telluride. Later, these early formed Au-Ag tellurides are replaced by Te-Bi minerals, mainly kochkarite, rucklidgeite and volynskite.

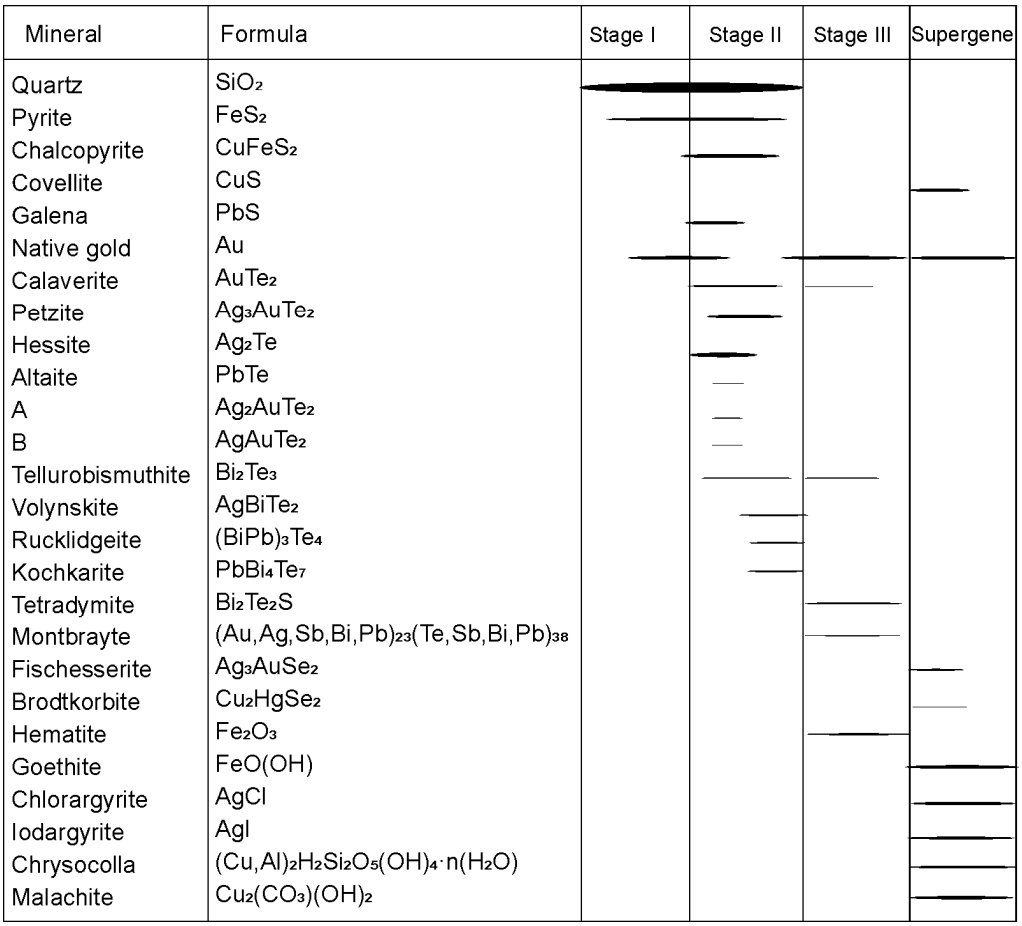

Figure 9. Paragenetic sequence in the San Luis Alta deposit.

In the third stage, a fracturing event produces new fractures that are filled with hematite, and this also partially replaces pyrite. Gold and Bi tellurides also precipitated, and this is associated with this event. Gold occurs as native gold and calaverite. Finally, the precipitation of tellurobismuthite, tetradymite and montbrayite is produced.

The supergene stage is characterized by alteration minerals with goethite, chrysocolla, malachite, chlorargyrite and iodargyrite. Tellurides are absent, but selenides rarely precipitate as fischesserite and brodtkorbite. Gold is precipitated as porous or mustard gold and also in euhedral crystals.

5. Discussion

The mineralogy of gold-bearing associations varies in the different gold deposits of the Nazca-Ocoña belt. Crespo et al. [23] only found bismuthine and some coloradoite crystals, as the only Te phase. In the case of Misky, it is also scarce in tellurides and, although bismuth is relatively abundant, it only appears as bismuthine, and very rarely as cuprobismutite. In the San Cristóbal deposit, tsumoite has been found in sparse crystals included in pyrite.

In all these cases, the Au mineralization starts from a composition dominated by gold and poor in silver. Even in San Luis, the first generation of pyrite has no tellurides. This suggests that the Te fugacity of the fluids that form these deposits was low. However, while in some deposits it became relatively high in intermediate stages, in others, it remained low, which explains the abundance of electrum in the fracture precipitation of the previously formed sulfides. In contrast, in other deposits such as San Luis, the increase in Te fugacity favored gold scavenging from the hydrothermal fluid and exsolved a Bi, Te melt that can effectively extract Au from these fluids [1,6,43]. Then, when the silver content increases,

it precipitates as Au-Ag tellurides, instead of electrum formation. This occurs in a stage prior to fracturing, as evidenced by the presence of blebs in the pyrite (Figure 10). In this case, bismuth is combined with Te to form Bi tellurides instead of bismuthine. This could be indicative of the high Te fugacity.

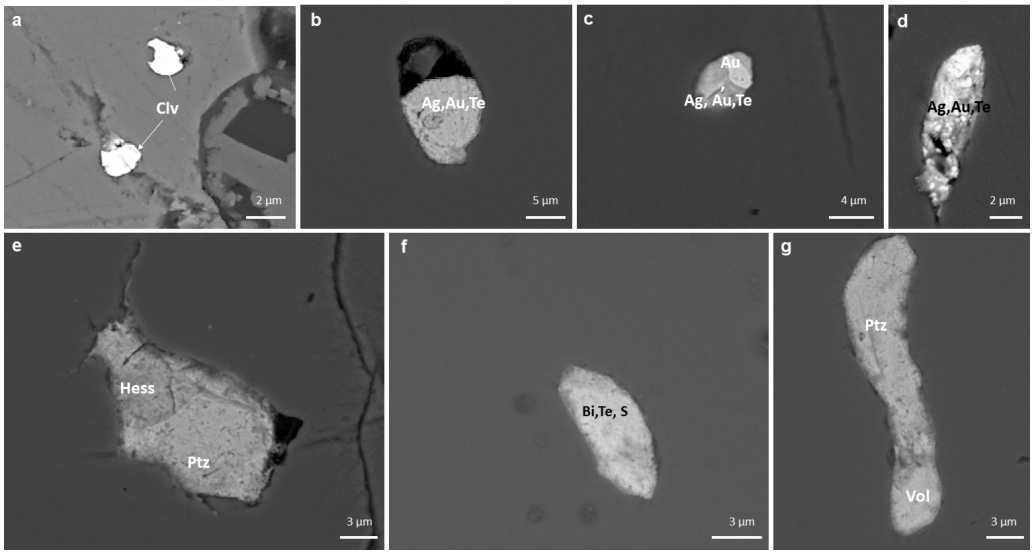

Figure 10. SEM images of the Au-Ag-Te-Bi associations from San Luis Alta as blebs included in pyrite: (**a**) calaverite; (**b**) partly filled inclusion with Ag-Au-Te mineralization; (**c**) Ag-Au-Te and Au grains; (**d**) Ag, Au, Te elongated inclusion; (**e**) hessite and petzite associated in a void with porosity; (**f**) small inhomogeneous inclusion of Bi-Te-S; (**g**) bleb of petzite and volynskite.

Later, a fracturing of the previously formed pyrite was produced and these Bi-Te minerals, such as tellurobismuthite and tetradymite, precipitated along with them. It is also worth mentioning the absence of Sb and As sulfosalts in San Luis, which contrasts with other deposits in the Nazca-Ocoña belt [23] and also with other deposits rich in Bi and Te, where bismuthine and Sb sulfosalts are abundant [16,44].

In the second half of the stage II, the fO_2 is relatively low and fluids are at least slightly acidic, according to the stability pH-log aO_2 diagrams of the Te-Au-Ag-Bi minerals [6]. The presence of a gold rim around Bi and Te ores is common and can be justified by the action of the Bi-Te-rich melts as Au scavengers. The Bi- and Te-rich melts would facilitate the dissolution of previously formed gold, which would be partially incorporated into the new Bi and Te minerals [45]. Other deposits where this process has been considered are rich in bismuthinite [41] or bismuthinite and native bismuth [46] and this was also confirmed by experimental work [47,48]. The absence of these minerals and abundance of tellurobismuthite could be attributed to the high Te content of the formation fluids of the San Luis deposit. The spherical and curved textures in blebs (Figure 10) agree with precipitation from a melt [49,50]. This high Te fugacity would lead to a high Te/S ratio, which explains the lack of sulfides other than pyrite in this third stage. In the Bi-poor deposits of the Nazca Ocoña belt, abundant galena appears in the fracture stage. In contrast, in San Luis, galena and chalcopyrite occur in small quantities together with hessite and petzite and do not re-form. In Bi, Te-rich stages Pb is associated with these elements forming altaite, kochkarite and rucklidgeite. This can be explained because in the presence of Te-Bi melts Pb would be fractionated from the hydrothermal fluid to the melt phase [51].

Finally, oxidation occurs extensively, giving rise to hematite veins and the replacement of pyrite in some places by hematite and chalcopyrite by covellite. This event is particularly intense in the San Luis, Santa Filomena, Cháparra and Mollehuaca deposits. Associated with this event, abundant silver chlorides and selenides such as fischesserite precipitate. Gold, in this case, is often associated with chlorargyrite and iodargyrite and precipitates in this phase in the form of mustard gold, with negligible Ag contents. The absence of Ag agrees with the supergene origin of gold; thus, during weathering, the Ag component is unstable and forms chlorargyrite [31,52].

6. Conclusions

Gold mineralization in some veins of the San Luis Alta deposit is accompanied by tellurides. These are initially calaverite, petzite and hessite. Bismuth tellurides are also formed, such as volynskite, rucklidgeite and tellurobismuthite. This mineralization often occurs in equilibrium as blebs hosted in pyrite and apparently crystallized from a melt exsolved from the Te- and Bi-rich hydrothermal fluids. This melt scavenged Au from the fluid and finally precipitated together with the Bi-Te minerals. At a later stage, tetradymite is formed, which mainly fills fractures in pyrite.

In later stages, the fO_2 increased and Fe oxides were formed. These oxides crosscut the sulfide mineralization; Au precipitated in this late stage, often as mustard gold, and very rarely as selenides such as fischesserite and brodtkorbite.

A late generation of gold associated with chlorargyrite and iodargyrite is produced when the deposit is subjected to supergene alteration.

The results obtained in this study show that the different deposits of the Palpa-Nazca-Ocoña belt must be processed in different ways for optimum gold recovery. In the case of San Luis Alta, a pre-cyanidation treatment must be carried out.

Author Contributions: Conceptualization: P.A.; fieldwork: P.A., E.C., A.M., M.T.Y., N.S.-R. and H.A.; methodology and analysis: P.A., M.G.-V. and A.M.; writing—original draft preparation: P.A.; writing—review and editing: P.A., H.A. and N.S.-R.; project administration, P.A.; funding acquisition, P.A. and M.G.-V. All authors have read and agreed to the published version of the manuscript.

Funding: This research was partially funded by the Generalitat de Catalunya (Autonomous Government of Catalonia) to the Consolidated Research Groups SGR 01041 (RIIS) and SGR 0026 (GEOXiS) and the CCD projects 2017-O013 and 2019-B005.

Data Availability Statement: The data presented in this study are available upon request from the corresponding author.

Acknowledgments: Technical assistance was kindly provided by Xavier Llovet (EPMA) of them at the Centres Científics i Tecnològics of the Universitat de Barcelona. We are grateful to the Cooperativa Minera-Artesanal San Luis, S.A. for their cooperation during the sampling. The manuscript was improved through reviews from the Academic Editor, and two anonymous reviewers. We thank the editorial staff of *Minerals* for their task.

Conflicts of Interest: The authors declare no conflict of interest.

References

1. Ciobanu, C.L.; Cook, N.J.; Pring, A. Bismuth tellurides as gold scavengers. In *Mineral Deposit Research: Meeting the Global Challenge*; Mao, J.W., Bierlein, F.P., Eds.; Springer: Berlin/Heidelberg, Germany; New York, NY, USA, 2005; pp. 1383–1386.
2. Ciobanu, C.L.; Cook, N.J.; Spry, P.G. Preface-Special Issue: Telluride and selenide minerals in gold deposits-how and why? *Mineral. Petrol.* **2006**, *87*, 163. [CrossRef]
3. Yin, C.; Liu, J.; Carranza, E.J.M.; Zhai, D.; Guo, Y. Mineralogical constraints on the genesis of the Dahu quartz vein-style Au-Mo deposit, Xiaoqinling gold district, China: Implications for phase relationships and physicochemical conditions. *Ore Geol. Rev.* **2019**, *113*, 103107. [CrossRef]
4. Weng, G.; Liu, J.; Carranza, E.J.M.; Zhai, D.; Zhang, F.; Wang, Y.; Yu, C.; Zhang, B.; Liu, X.; Sun, B.; et al. Mineralogy and geochemistry of tellurides, selenides and sulfides from the Zhaishang gold deposit, western Qinling, China: Implications for metallogenic processes. *J. Asian Earth Sci.* **2023**, *244*, 105536. [CrossRef]

5. Zhai, D.; Liu, J. Gold-telluride-sulfide association in the Sandaowanzi epithermal Au-Ag-Te deposit, NE China: Implications for phase equilibrium and physicochemical conditions. *Miner. Pet.* **2014**, *108*, 853–871. [CrossRef]
6. Cook, N.J.; Ciobanu, C.L.; Spry, P.G.; Voudouris, P. Understanding gold-(silver)–telluride-(selenide) mineral deposits. *Episodes* **2009**, *32*, 249–263. [CrossRef]
7. Spry, P.G.; Chryssoulis, S.; Ryan, C.G. Process mineralogy of gold: Gold from telluride-bearing ores. *Jom* **2004**, *56*, 60–62. [CrossRef]
8. Zhang, J.; Zhang, Y.; Richmond, W.; Wang, H.P. Processing technologies for gold-telluride ores. *Int. J. Miner. Met. Mater.* **2010**, *17*, 1–10. [CrossRef]
9. Alfonso, P.; Anticoi, H.; Yubero, T.; Bascompta, M.; Henao, L.; Garcia-Valles, M.; Palacios, S.; Yáñez, J. The importance of mineralogical knowledge in the sustainability of artisanal gold mining: A mid-south Peru case. *Minerals* **2019**, *9*, 345. [CrossRef]
10. Ellis, S. Treatment of gold-telluride ores. Developments in mineral processing. *Dev. Miner. Process.* **2005**, *15*, 973–984.
11. Zhao, Z.H.; Zhang, P.H.; Xiong, X.L.; Wang, Q. Au-Te deposits associated with alkali-rich igneous rocks in China. In *Mineral Deposit Research: Meeting the Global Challenge*; Mao, J.W., Bierlein, F.P., Eds.; Springer: Berlin/Heidelberg, Germany; New York, NY, USA, 2005; pp. 1451–1454.
12. Rodríguez-Terente, L.M.; Martin-Izard, A.; Arias, D.; Fuertes-Fuente, M.; Cepedal, A. The Salave Mine, a Variscan intrusion-related gold deposit (IRGD) in the NW of Spain: Geological context, hydrothermal alterations and ore features. *J. Geochem. Explor.* **2018**, *188*, 364–389. [CrossRef]
13. Shackleton, J.M.; Spry, P.G.; Bateman, R. Telluride mineralogy of the golden mile deposit, Kalgoorlie, Western Australia. *Can. Miner.* **2003**, *41*, 1503–1524. [CrossRef]
14. Roberts, J.A.; Groat, L.A.; Spry, P.G.; Cempírek, J. Telluride Mineralogy of the Deer Horn Au-Ag-Te-(Bi-Pb-W) Deposit, British Columbia: Implications for the Generation of Tellurides. *Can. Miner.* **2021**, *60*, 989–1011. [CrossRef]
15. Vikent'eva, O.V.; Prokofiev, V.Y.; Gamyanin, G.N.; Goryachev, N.A.; Bortnikov, N.S. Intrusion-related gold-bismuth deposits of North-East Russia: PTX parameters and sources of hydrothermal fluids. *Ore Geol. Rev.* **2018**, *102*, 240–259. [CrossRef]
16. Damdinov, B.B.; Huang, X.W.; Goryachev, N.A.; Zhmodik, S.M.; Mironov, A.G.; Damdinova, L.B.; Khubanov, V.B.; Reutsky, V.N.; Yudin, S.Y.; Travin, A.V.; et al. Intrusion-hosted gold deposits of the southeastern East Sayan (northern Central Asian Orogenic Belt, Russia). *Ore Geol. Rev.* **2021**, *139*, 104541. [CrossRef]
17. Vargas, A.R. *Estudio Geológico-Minero de la Faja Aurífera Nazca-Ocoña*; Technical Report; INGEMMET: Lima, Peru, 1978; p. 179.
18. Steinmüller, K. *Depósitos Metálicos en el Peru. Su Metalogénia, sus Modelos, su Exploración y el Medio Ambiente*; INGEMMET: Lima, Peru, 1999; p. 171.
19. Sillitoe, R.H. Epochs of intrusion-related copper mineralization in the Andes. *J. South Am. Earth Sci.* **1988**, *1*, 89–108. [CrossRef]
20. Sillitoe, R.H.; Thompson, J.F. Intrusion–Related Vein Gold Deposits: Types, Tectono-Magmatic Settings and Difficulties of Distinction from Orogenic Gold Deposits. *Resour. Geol.* **1998**, *48*, 237–250. [CrossRef]
21. Cardozo, M.; Cedillo, E. Geologic-metallogenetic evolution of the Peruvian Andes. In *Stratabound ore deposits in the Andes*; Springer: Berlin/Heidelberg, Germany, 1990; pp. 37–60.
22. Acosta, J. *Características Metalogénicas de los Yacimientos Asociados a los Arcos Magmáticos Mesozoicos y Cenozoicos del sur del Peru (Latitudes 16°–14° S)*; Technical Report; INGEMET: Lima, Peru, 2006; p. 24.
23. Crespo, J.; Holley, E.; Pfaff, K.; Guillen, M.; Huamani, R. Ore Mineralogy, Trace Element Geochemistry and Geochronological Constraints at the Mollehuaca and San Juan de Chorunga Au-Ag Vein Deposits in the Nazca-Ocoña Metallogenic Belt, Arequipa, Peru. *Minerals* **2020**, *10*, 1112. [CrossRef]
24. Cobbing, E.J.; Pitcher, W.S.; Taylor, W.P. Segments and super-units in the Coastal Batholith of Peru. *J. Geol.* **1977**, *85*, 625–631. [CrossRef]
25. Beckinsale, R.D.; Sanchez-Fernandez, A.W.; Brook, M.; Cobbing, E.J.; Taylor, W.P.; Moore, N.D. Rb-Sr whole-rock isochron and K-Ar age determinations for the Coastal Batholith of Peru. In *Magmatism at a Plate Edge. The Peruvian Andes*; Pitcher, W.S., Atherton, M.P., Cobbing, E.J., Beckinsale, R.D., Eds.; Blackie and Son: London, UK, 1985; pp. 177–202.
26. Acosta, J.; Quispe, J.; Rivera, R.; Valencia, M.; Chirif, H.; Huanacuni, D.; Rodríguez, I.; Villarreal, E.; Paico, D.; Santisteban, A. *Mapa Metalogenético del Oro en el Peru*; INGEMET: Lima, Peru, 2010.
27. Zhao, J.; Brugger, J.; Grundler, P.V.; Xia, F.; Chen, G.; Pring, A. Mechanism and kinetics of a mineral transformation under hydrothermal conditions: Calaverite to metallic gold. *Am. Mineral.* **2009**, *94*, 1541–1555. [CrossRef]
28. Shikazono, N.; Shimizu, M. The Ag/Au ratio of native gold and electrum and the geochemical environment of gold vein deposits in Japan. *Miner. Depos.* **1987**, *22*, 309–314. [CrossRef]
29. Zhao, J.; Pring, A. Mineral transformations in gold–(silver) tellurides in the presence of fluids: Nature and experiment. *Minerals* **2019**, *9*, 167. [CrossRef]
30. Tolstykh, N.D.; Palyanova, G.A.; Bobrova, O.G.V.; Sidorov, E.G. Mustard gold of the Gaching ore deposit (Maletoyvayam ore Field, Kamchatka, Russia). *Minerals* **2019**, *9*, 489. [CrossRef]
31. Bowell, R.J. Supergene gold mineralogy at Ashanti, Ghana: Implications for the supergene behaviour of gold. *Mineral. Mag.* **1992**, *56*, 545–560. [CrossRef]

32. Kalinin, A.A.; Savchenko, Y.E.; Selivanova, E.A. Mustard Gold in the Oleninskoe Gold Deposit, Kolmozero–Voronya Greenstone Belt, Kola Peninsula, Russia. *Minerals* **2019**, *9*, 786. [CrossRef]
33. Townley, B.K.; Hérail, G.; Maksaev, V.; Palacios, C.; Parseval, P.; Sepúlveda, F.; Orellana, R.; Rivas, P.; Ulloa, C. Gold grain morphology and composition as an exploration tool: Application to gold exploration in covered areas. *Geochemistry: Explor. Environ. Anal.* **2003**, *3*, 29–38. [CrossRef]
34. Cabri, L.J. Phase relations in the Au-Ag-Te systems and their mineralogical significance. *Econ. Geol.* **1965**, *60*, 1569–1606. [CrossRef]
35. Xu, H.; Yu, Y.; Wu, X.; Yang, L.; Tian, Z.; Gao, S.; Wang, Q. Intergrowth texture in Au-Ag-Te minerals from Sandaowanzi gold deposit, Heilongjiang Province: Implications for ore-forming environment. *Chin. Sci. Bull.* **2012**, *57*, 2778–2786. [CrossRef]
36. Cook, N.J.; Ciobanu, C.L. Paragenesis of Cu-Fe ores from Ocna de Fier-Dognecea (Romania), typifying fluid plume mineralization in a proximal skarn setting. *Miner. Mag.* **2001**, *65*, 351–372. [CrossRef]
37. Maslennikov, V.V.; Maslennikova, S.P.; Large, R.R.; Danyushevsky, L.V.; Herrington, R.J.; Stanley, C.J. Tellurium-bearing minerals in zoned sulfide chimneys from Cu-Zn massive sulfide deposits of the Urals, Russia. *Miner. Petrol.* **2013**, *107*, 67–99. [CrossRef]
38. Savva, N.E.; Pal'Yanova, G.A.; Byankin, M.A. The problem of genesis of gold and silver sulfides and selenides in the Kupol deposit (Chukotka, Russia). *Russ. Geol. Geophys.* **2012**, *53*, 457–466. [CrossRef]
39. Kuzhuget, R.V.; Ankusheva, N.N.; Pirajno, F.; Mongush, A.A.; Butanaev, Y.V.; Suge-Maadyr, N.V. The Ulug-Sair Gold Occurrence (Western Tuva, Russia): Mineralogy, Ore Genesis, and SO Isotope Systematics. *Minerals* **2022**, *12*, 712. [CrossRef]
40. Marquez Zavalia, M.F.; Galliski, M.A.; Skacha, P.; Macek, I.; Sejkora, J.; Dolnícek, Z. Mineralogy of the Rincon Blanco selenide occurrence, La Rioja, Argentina. *J. Geosci.* **2021**, *66*, 1–14. [CrossRef]
41. Škácha, P.; Sejkora, J.; Plášil, J. Selenide mineralization in the Příbram uranium and base-metal district (Czech Republic). *Minerals* **2017**, *7*, 91. [CrossRef]
42. Liu, J.; Wang, Y.; Huang, S.; Wei, R.; Sun, Z.; Hu, Q.; Hao, J. The gold occurrence in pyrite and Te–Bi mineralogy of the Fancha gold deposit, Xiaoqinling gold field, southern margin of the North China Craton: Implication for ore genesis. *Geol. J.* **2020**, *55*, 5791–5811. [CrossRef]
43. Bi, S.J.; Li, J.W.; Zhou, M.F.; Li, Z.K. Gold distribution in As-deficient pyrite and telluride mineralogy of the Yangzhaiyu gold deposit, Xiaoqinling district, southern North China craton. *Miner. Deposita* **2011**, *46*, 925–941. [CrossRef]
44. Feng, H.; Shen, P.; Zhu, R.; Tomkins, A.G.; Brugger, J.; Ma, G.; Li, C.; Wu, Y. Bi/Te control on gold mineralizing processes in the North China Craton: Insights from the Wulong gold deposit. *Miner. Deposita* **2003**, *58*, 263–286. [CrossRef]
45. Ciobanu, C.L.; Birch, W.D.; Cook, N.J.; Pring, A.; Grundler, P.V. Petrogenetic significance of Au–Bi–Te–S associations: The example of Maldon, Central Victorian gold province, Australia. *Lithos* **2010**, *116*, 1–17. [CrossRef]
46. Cockerton, A.B.; Tomkins, A.G. Insights into the liquid bismuth collector model through analysis of the Bi-Au Stormont skarn prospect, northwest Tasmania. *Econ. Geol.* **2012**, *107*, 667–682. [CrossRef]
47. Tooth, B.; Brugger, J.; Ciobanu, C.L.; Liu, W. Modeling of gold scavenging by bismuth melts coexisting with hydrothermal fluids. *Geochim. Cosmochim. Acta* **2011**, *75*, 5423–5443. [CrossRef]
48. Tooth, B.; Ciobanu, C.L.; Green, L.; O'Neill, B.; Brugger, J. Bi-melt formation and gold scavenging from hydrothermal fluids: An experimental study. *Geology* **2008**, *36*, 815–818. [CrossRef]
49. Ciobanu, C.L.; Cook, N.J.; Damian, F.; Damian, G. Gold scavenged by bismuth melts: An example from Alpine shear-remobilizates in the Highiş Massif, Romania. *Mineral. Petrol.* **2006**, *87*, 351–384. [CrossRef]
50. Zhou, H.; Sun, X.; Cook, N.J.; Lin, H.; Fu, Y.; Zhong, R.; Brugger, J. Nano-to micron-scale particulate gold hosted by magnetite: A product of gold scavenging by bismuth melts. *Econ. Geol.* **2017**, *112*, 993–1010. [CrossRef]
51. Cave, B.J.; Barnes, S.J.; Pitcairn, I.K.; Sack, P.J.; Kuikka, H.; Johnson, S.C.; Duran, C.J. Multi-stage precipitation and redistribution of gold, and its collection by lead-bismuth and lead immiscible liquids in a reduced-intrusion related gold system (RIRGS); Dublin Gulch, western Canada. *Ore Geol. Rev.* **2019**, *106*, 28–55. [CrossRef]
52. Krupp, R.E.; Weiser, T. On the stability of gold-silver alloys in the weathering environment. *Miner. Deposita* **1992**, *27*, 268–275. [CrossRef]